Dual Scattering Approximation for Fast Multiple Scattering in Hair

Arno Zinke*
Institut für Informatik II
Universität Bonn

Cem Yuksel†
Dept. of Computer Science
Texas A&M University

Andreas Weber‡
Institut für Informatik II
Universität Bonn

John Keyser§
Dept. of Computer Science
Texas A&M University

Path tracing (7.8 hours) | Offline **dual scattering** (5.2 minutes) | Real-time **dual scattering** (14 fps)

Using only single scattering (20 fps) | Single scattering + diffuse (20 fps) | Kajiya-Kay shading model (20 fps)

Figure 1: *Comparison of our method to path tracing and existing hair shading methods with deep opacity maps. Our dual scattering approximations (offline ray shooting and real-time GPU-based implementations) achieve close results to the path tracing reference without any parameter adjustment and with significantly improved rendering times. Using single scattering only fails to produce the correct hair color. Adding an ad-hoc diffuse component or Kajiya-Kay shading model also fails to achieve the same realism, even after hand tweaking the diffuse color and shadow opacity to match the reference. The hair model has 50K strands and 1.4M line segments.*

Abstract

When rendering light colored hair, multiple fiber scattering is essential for the right perception of the overall hair color. In this context, we present a novel technique to efficiently approximate multiple fiber scattering for a full head of human hair or a similar fiber based geometry. In contrast to previous ad-hoc approaches, our method relies on the physically accurate concept of the Bidirectional Scattering Distribution Functions and gives physically plausible results with no need for parameter tweaking. We show that complex scattering effects can be approximated very well by using aggressive simplifications based on this theoretical model. When compared to unbiased Monte-Carlo path tracing, our approximations preserve photo-realism in most settings but with rendering times at least two-orders of magnitude lower. Time and space complexity are much lower compared to photon mapping-based techniques and we can even achieve realistic results in real-time on a standard PC with consumer graphics hardware.

CR Categories: I.3.7 [Computer Graphics]: Three-Dimensional Graphics and Realism—Color, shading, shadowing, and texture

Keywords: Hair rendering, multiple scattering, GPU algorithms

*e-mail: zinke@cs.uni-bonn.de
†e-mail: cem@cemyuksel.com
‡e-mail: weber@cs.uni-bonn.de
§e-mail: keyser@cs.tamu.edu

1 Introduction

Accounting for multiple scattering is a key factor in the realistic rendering of human hair. Particularly in dense, light-colored hair, multiple scattering provides a critical component of the hair color, similar to the effect seen in subsurface scattering of translucent materials. Unfortunately, the high geometric complexity of hair

models coupled with the complexity of the light interaction in hair volumes makes computing this multiple scattering effect difficult. Even for the simplest case of computing illumination due to a single point light source, contributions of several different light paths need to be determined to achieve reasonable visual accuracy.

Recently, two different photon mapping based methods have been proposed to accelerate the multiple scattering computation in hair. Even though these methods present a significant speed improvement as compared to brute force path tracing, they still require hours to compute a single frame and a large amount of memory to store the photon map. On the other hand, in real-time graphics the multiple scattering property of hair is overly simplified and treated as transparent shadows (completely ignoring the effect of the circular shape of hair fibers) coupled with an ad-hoc diffuse component. This extreme simplification prevents the use of physically based hair shaders, and gives hair a dull appearance. Furthermore, rigorous parameter tweaking is necessary to achieve acceptable results, the realism of which is always questionable.

In this paper, we introduce the concept of dual scattering, which splits the multiple scattering computation into two components: *global multiple scattering* and *local multiple scattering*. The global multiple scattering component aims to compute the light traveling through the hair volume and reaching the neighborhood of the point of interest, while local multiple scattering accounts for the scattering events within this neighborhood. Exploiting physically based scattering properties of real hair fibers, we introduce several theoretical simplifications for computing both of these components; this permits extremely efficient multiple scattering computations with minimal accuracy compromise. As a result of our aggressive theoretical simplifications, the implementation of global multiple scattering becomes very similar to standard semi-transparent hair shadowing techniques, while local multiple scattering is modeled as a material property derived from hair fiber properties.

The top row of Figure 1 compares different implementations of our dual scattering method to path tracing. The path tracing image takes 7.8 hours to compute, while by using dual scattering we can reduce this time to 5.2 minutes in our offline implementation or even 14 frames per second with our GPU implementation. The precomputation time required for all dual scattering implementations is only a few seconds. As can be seen from these images, we can maintain visual accuracy with significant improvement in computation time. Just as important, all calculations are based on computable or measurable values, so there is no unintuitive parameter tweaking (such as smoothing radius) that existed in previous physically based techniques.

The bottom row of Figure 1 shows the results of single scattering only and existing hair shading methods with semi-transparent shadows using deep opacity maps. Even after rigorous parameter tweaking of ad-hoc diffuse color used by the shaders and the opacity value used for the shadow computation, the results still differ significantly from the path tracing reference. This is mainly because several important multiple scattering effects like directionality, color shifts, and successive blurring cannot be modeled by these oversimplified formulations. Therefore, the realism that we achieve using our dual scattering approximation goes beyond existing real-time hair rendering methods. Note that dual scattering is not an ad-hoc addition for enhancing real-time hair rendering; it is a physically-based simulation, the simplicity of which permits real-time implementation.

In the next section we provide a brief summary of the previous work and the terminology we use throughout the paper. The theory of dual scattering is introduced in Section 3. We present the details of our different implementations in Section 4 and our results in Section 5. Finally, we conclude with a short discussion in Section 6.

2 Background

There is a large body of work on hair modeling and rendering in computer graphics. In this section we only review the techniques that are most relevant to our approach and we concentrate on physically based methods. For a more comprehensive overview of hair rendering please refer to the recent survey paper of Ward et al. [2007].

2.1 Prior Work

Marschner et al. [2003] presented the seminal work in the physically-based rendering of human hair. Their paper developed a far-field scattering model for hair based on measurements of actual hair. They modeled hair fibers as dielectric cylinders with colored interiors, and their model was able to account for important single scattering effects, such as multiple highlights, and deliver realistic results for dark colored hair.

Further work showed that multiple fiber scattering is essential for correct perception of hair color, particularly for light colored hair. New models [Zinke et al. 2004; Moon and Marschner 2006; Zinke and Weber 2007] were developed to generalize the approach of Marschner et al. [2003] to account for these multiple scattering effects.

In order to solve this more general illumination problem, methods such as path tracing can be used, though this often leads to prohibitive running times. Both Moon and Marschner [2006] and Zinke and Weber [2006] use photon mapping approaches to estimate the multiple scattering. Although both methods can produce accurate results similar to path tracing in many situations, they are computationally costly and require high resolution (memory consuming) photon maps. These methods cannot be made interactive. Yuksel et al. [2007] have also proposed an alternative projection-based method for rendering global illumination for fibers. However, this approach makes several simplifications, e.g. neglecting inter-reflections, that reduce accuracy.

A number of other techniques have addressed some aspects of multiple scattering effects for hair volumes, especially in the context of self-shadowing for interactive hair rendering [Lokovic and Veach 2000; Kim and Neumann 2001; Mertens et al. 2004; Bertails et al. 2005; Xu et al. 2006; Hadwiger et al. 2006; Yuksel and Keyser 2008]. However, the main drawback of most of these methods is that they use ad-hoc simplifications and non-physical parameters, which cannot be derived from physical hair fiber properties. While plausible images can be produced by these methods in some situations, parameters need to be repeatedly tweaked to be appropriate for a particular scene and lighting condition. An exception is the work of Gupta and Magnenat-Thalmann [2005], which provides a more complex scattering-based approach. However, their approach is purely density-based and uses an ad-hoc volumetric scattering function without any physical basis. Therefore it cannot capture important phenomena such as directionality of multiple scattering, successive blurring, or subtle color shifting effects.

For simulating volumetric light transport, cheap analytical multiple scattering models have been presented [Kniss et al. 2003; Premoze et al. 2004]. By taking into account optical properties of a participating media Premoze et al. [2004] use practical approximations to efficiently compute important features of multiply scattered light, such as spatial and angular spread of an incident beam. The radiative transfer is computed based on only a few prototypic path samples. However, even though this work is related in spirit to our approach, it has not yet been demonstrated to work with spatially varying and highly anisotropic scattering of hair fibers.

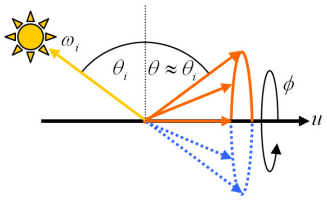

Figure 2: *Definition of angles and directions*

2.2 Terminology and Notation

The discussion in this paper includes numerous symbols and terms that might not be familiar to readers. We follow the terminology and notation used by Marschner et al. [2003] and Zinke and Weber [2007]. While we would refer the reader to those sources for more complete descriptions, we give a brief review and overview of terminology here.

Referring to Figure 2, consider the tangent to the hair fiber (i.e. a vector running down the central fiber axis), u. The normal plane is the plane perpendicular to u. Directions within this normal plane are referred to as *azimuthal* angles, and are expressed with the symbol ϕ. An angle formed with respect to the normal plane is called the *longitudinal* inclination, and is expressed with the symbol θ. For a point on the fiber, a direction is expressed by the symbol ω. Thus, any direction ω_a is equivalently expressed by the longitudinal inclination θ_a and the azimuthal angle ϕ_a.

The amount of incoming light from one given direction, ω_i, scattered in another given outgoing direction, ω_o, is expressed by a Bidirectional Scattering Distribution Function. For a hair fiber, Zinke and Weber [2007] defined a very general Bidirectional Fiber Scattering Distribution Function that incorporated fiber geometry in addition to incident and output angles. By assuming the viewer and light source are sufficiently far from the hair fiber, one can ignore the hair geometry and local (near-field) variations in geometry, resulting in a simplified Bidirectional Curves Scattering Distribution Function (BCSDF), $f_s(\omega_i, \omega_o)$. The scattering function defined by Marschner et al. [2003] is one possible BCSDF.

A hair fiber is generally thought of as a cylinder, and as light hits these cylinder boundaries, it can either be transmitted (T) or reflected (R). Thus, TT refers to the light passing into then out of the fiber in a generally forward direction, while R and TRT refer to backward reflections, either before (R) or after (TRT) passing through the fiber. Computing a BCSDF generally involves computing these three components, and more complex interactions (e.g. TRRT) are ignored.

We follow both Marschner et al. [2003] and Zinke and Weber [2007] in using a formulation for the BCSDF as a product of a longitudinal function, M_t, and an azimuthal function, N_t for each of the three reflection types $t \in (\mathrm{R}, \mathrm{TT}, \mathrm{TRT})$. M is modeled as a normalized Gaussian function $g(\alpha_t, (\beta_t)^2)$ with mean α_t and standard deviation β_t specified according to measured properties of hairs. N is precomputed in a 2D table of difference angles $\theta = (\theta_o - \theta_i)/2$ and $\phi = \phi_o - \phi_i$. See Marschner et al.'s paper [2003] for more details on these computations. Note that in this paper, $g(a, b)$ refers to a unit area Gaussian function defined in variable a with a zero mean and variance b.

3 Dual Scattering

In this section we present the theoretical foundations of the dual scattering approximation. We simplify the computation of the complicated physical multiple scattering phenomena using properties of real human hair fibers and realistic human hair models. As a result of these simplifications, we achieve a physically-based formulation for multiple scattering, which can be implemented in a very similar way to standard hair shadowing techniques.

Similar to Moon and Marschner [2006], in our rendering system we use one dimensional fibers, disregarding the illumination variation across the width of a hair strand. In this form, the general rendering equation for outgoing radiance L_o towards a direction ω_o at a point x can be written as

$$L_o(x, \omega_o) = \int_\Omega L_i(x, \omega_i)\, f_s(\omega_i, \omega_o)\, \cos\theta_i \, \mathrm{d}\omega_i \ , \qquad (1)$$

where $L_i(x, \omega_i)$ is the incident radiance from direction ω_i, $f_s(\omega_i, \omega_o)$ is the BCSDF of a hair fiber, and Ω is the set of all directions over the sphere. The incident radiance function $L_i(x, \omega_i)$ includes all light paths scattered inside the hair volume such that

$$L_i(x, \omega_i) = \int_\Omega L_d(\omega_d)\, \Psi(x, \omega_d, \omega_i)\, \mathrm{d}\omega_d \ , \qquad (2)$$

where $L_d(\omega_d)$ is the incoming radiance from outside the hair volume from direction ω_d (assuming distant illumination), and $\Psi(x, \omega_d, \omega_i)$ is the *multiple scattering function* denoting the fraction of light entering the hair volume from direction ω_d that is scattered inside the hair volume and finally arriving at point x from direction ω_i.

The main concept behind the dual scattering method is to approximate the multiple scattering function as a combination of two components: *global multiple scattering* and *local multiple scattering*. The global multiple scattering function Ψ^G is used to compute the irradiance arriving at the neighborhood of a point x inside the hair volume, and the local multiple scattering function Ψ^L approximates the multiple scattering of this irradiance within the local neighborhood of x (Figure 3). Therefore, the multiple scattering function becomes the sum of global multiple scattering and global multiple scattering that goes through further local multiple scattering

$$\Psi(x, \omega_d, \omega_i) = \Psi^G(x, \omega_d, \omega_i)\, \left(1 + \Psi^L(x, \omega_d, \omega_i)\right) \ . \qquad (3)$$

For the sake of simplicity we explain our dual scattering method assuming that the subject hair model is illuminated by a single directional light source. At the end of this section we explain how this approach can be extended for other light source types, multiple light sources, image based lighting, and global illumination.

3.1 Global Multiple Scattering

Global multiple scattering is especially important for light colored hair types as they permit outside illumination to penetrate

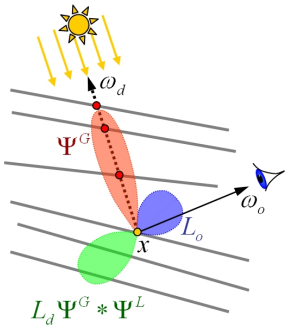

Figure 3: *Based on intersections (red dots) along the shadow path (dashed line), the multiple scattering distributions Ψ_L and Ψ_G and the resulting outgoing radiance L_o are locally estimated.*

deeper into the hair volume. According to the measurements of Marschner et al. [2003], light scattering from human hair fibers is strongly anisotropic in the longitudinal direction, while it is much less anisotropic in the azimuthal direction. Because of this rather wide azimuthal scattering property of human hair, the computation of global multiple scattering should handle several different rather complicated light paths. On the other hand, the energy of light arriving at a point does not depend on the actual path, but the quality of the scattering events along the path. Assuming statistically independent scattering events, all other geometrical properties of the cluster (such as the distance between fibers) can be neglected. Moreover, a realistic human hair model presents strong local similarity in the orientation of neighboring hair fibers, therefore the probabilities of different light paths exhibit this similarity.

Based on these observations, in our dual scattering method we simplify the computation of global multiple scattering by exploring the light scattering properties along only a single light path, namely the *shadow path* (in the direction ω_d), and use the information we gather for approximating the contributions of other possible paths (Figure 3). Along the shadow path, we classify all possible scattering directions of a scattering event into two groups: *Forward Scattering* and *Backward Scattering*, which correspond to all directions in the front and back half of the scattering cone relative to the original light source.

Note that the strong TT component of hair fiber scattering is included in the front half-cone. Therefore, for light colored hair models forward scattering is significantly stronger than backward scattering. Furthermore, light paths that go through a backward scattering before reaching the neighborhood of point x scatter away from this point, and they need another backward scattering to reverse their direction. As a result, for light colored hair types only a very small portion of global multiple scattering includes backward scattering. In our formulation we disregard these double (or more) backward scattered paths, approximating the global multiple scattering by only front scattered radiance. (Note that backward scattered paths are ignored only for the global multiple scattering computation and they will be included in local multiple scattering). As a result, we approximate the global multiple scattering as

$$\Psi^G(x, \omega_d, \omega_i) \approx T_f(x, \omega_d)\, S_f(x, \omega_d, \omega_i)\ , \tag{4}$$

where $T_f(x, \omega_d)$ is the total transmittance and $S_f(x, \omega_d, \omega_i)$ accounts for the spread of global multiple scattering into different directions. Therefore, to compute the global multiple scattering we need to evaluate these two functions.

3.1.1 Forward Scattering Transmittance

The transmittance function $T_f(x, \omega_d)$ gives the total attenuation of a front scattered light path arriving at the point x. Therefore, the transmittance function depends on the number of scattering events n along the shadow path and the average attenuation $\bar{a}_f(\theta_d)$ caused by each forward scattering event as

$$T_f(x, \omega_d) = d_f(x, \omega_d) \prod_{k=1}^{n} \bar{a}_f\big(\theta_d^k\big)\ , \tag{5}$$

where $d_f(x, \omega_d)$ is the density factor and θ_d^k is the longitudinal inclination at the k^{th} scattering event. Note that if $n = 0$, the point x is illuminated directly and the transmittance function is set to 1. We use the density factor $d_f(x, \omega_d)$ to account for the fact that not all points x are located inside a dense cluster. Thus, the front scattered irradiance on x comes from only a subset of all directions as shown in Figure 4. Although the density factor theoretically depends on the hair density and the specific location of x, in practice we simply use a constant value (between 0 and 1) to approximate this factor based on the overall hair density. In our experiments we found that for realistic human hair models density factors between 0.6 and 0.8 give realistic results (as compared to a path tracing reference). For all examples in this paper, the density factor is set to 0.7.

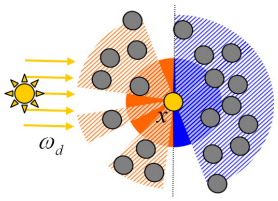

Figure 4: *Cross section of a hair cluster. The fiber at x is not fully surrounded by other strands, so it can receive multiple scattered radiance only from the shaded sections. d_f accounts for fibers in the orange region, while d_b accounts for fibers in the blue region.*

We compute the average attenuation $\bar{a}_f(\theta_d)$ directly from the fiber scattering function f_s as the total radiance on the front hemisphere due to isotropic irradiance along the specular cone:

$$\bar{a}_f(\theta_d) = \frac{1}{\pi} \int_{\Omega_f} \int_{-\frac{\pi}{2}}^{\frac{\pi}{2}} f_s\left((\theta_d, \phi), \omega\right) \cos\theta_d \, \mathrm{d}\phi \, \mathrm{d}\omega, \tag{6}$$

where Ω_f is all directions over the front hemisphere and θ_d is the inclination of direct illumination at the scattering event.

3.1.2 Forward Scattering Spread

The spread function $S_f(x, \omega_d, \omega_i)$ approximates the final angular distribution of front scattered light to find the probability of radiance coming to the point x from direction ω_i. Because of the wide azimuthal scattering property of hair fibers, front scattered radiance quickly becomes almost isotropic in the azimuthal direction after only a few scattering events. However, in the longitudinal direction front scattered spread is still rather anisotropic. Therefore, we represent our spread function using a constant term $\tilde{s}_f$ for the azimuthal spread and a narrow Gaussian distribution function g for the longitudinal component:

$$S_f(x, \omega_d, \omega_i) = \frac{\tilde{s}_f(\phi_d, \phi_i)}{\cos\theta_d}\, g\Big(\ \theta_d + \theta_i\ ,\ \bar{\sigma}_f^2(x, \omega_d)\ \Big)\ , \tag{7}$$

where $\tilde{s}_f(\phi_d, \phi_i)$ is $1/\pi$ for forward scattering directions and zero for backward scattering, and $\bar{\sigma}_f^2(x, \omega_d)$ is the total variance of forward scattering in the longitudinal directions. Since the BCSDF of a fiber is represented by a Gaussian distribution (M) in longitudinal directions, we can compute the total variance as the sum of variances of all scattering events along the shadow path

$$\bar{\sigma}_f^2(x, \omega_d) = \sum_{k=1}^{n} \bar{\beta}_f^2\big(\theta_d^k\big)\ , \tag{8}$$

where $\bar{\beta}_f^2(\theta_d^k)$ is the average longitudinal forward scattering variance of the k^{th} scattering event, which is directly taken from the BCSDF of the hair fiber. Note that for a single directional light source when $n = 0$, i.e. when the fiber is being illuminated directly, the spread function becomes a delta function $\delta(\omega_d - \omega_i)$.

3.2 Local Multiple Scattering

The local multiple scattering function accounts for the multiple scattering events within the neighborhood of the point x. Since light paths that go through only forward scattering are included in

the global multiple scattering function, light paths of the local multiple scattering function must include at least one backward scattering. Because of this backward scattering, local multiple scattering is mostly smooth with subtle changes over the hair volume, yet it significantly affects the visible hair color especially for light colored hair types.

In our dual scattering method, we combine local multiple scattering and the BCSDF of the hair fibers, approximating the result with a density factor d_b and backscattering function f_{back} as

$$\Psi^L(x, \omega_d, \omega_i)\, f_s(\omega_i, \omega_o) \approx d_b(x, \omega_d)\, f_{\text{back}}(\omega_i, \omega_o)\ . \quad (9)$$

Similar to forward scattering density factor d_f, backward scattering density factor d_b accounts for the hair density around the point x, and in practice we approximate it using a constant density term equal to d_f, which we set to 0.7. Note that f_{back} is not a function of x, which means that it is modeled as a material property. We formulate f_{back} as a product of an average backscattering attenuation function, $\bar{A}_b$, and an average spread function, $\bar{S}_b$, estimating the bidirectional multiple backscattering distribution function of a hair cluster as

$$f_{\text{back}}(\omega_i, \omega_o) = \frac{2}{\cos\theta}\ \bar{A}_b(\theta)\ \bar{S}_b(\omega_i, \omega_o)\ , \quad (10)$$

where $\theta = (\theta_o - \theta_i)/2$ is the difference angle of incident and outgoing inclinations and an additional $\cos\theta$ factor accounts for the fact that light is roughly scattered to a cone as in [Marschner et al. 2003]. To evaluate the effect of local multiple scattering we need to compute average backscattering attenuation $\bar{A}_b(\theta)$ and average backscattering spread $\bar{S}_b(\omega_i, \omega_o)$. Note that our formulation of Ψ^G and $\Psi^L f_s$ have a similar structure; however, these two expressions are conceptually different: Ψ^G models an angular radiance distribution whereas f_{back} serves as a curve scattering term (BCSDF).

3.2.1 Average Backscattering Attenuation

The average backscattering attenuation is computed for a point x inside a cluster of disciplined hair[1]. Since realistic hair models have strong similarity among neighboring hair strands, average attenuation computed for a disciplined hair cluster is a good approximation to be used in local multiple scattering. Furthermore, we ignore the slight change in the longitudinal inclination angle due to backward scattering events assuming that the absolute value of the longitudinal inclination $|\theta|$ is the same for all fibers in the cluster.

Local multiple scattering needs to account for the portion of light paths after they reach the neighborhood of point x. We consider only paths with an odd number of backward scattering events in this part of the light path. When there are an even number of backward scattering events in this part of the light path, the path points away from the light and does not return back to x; thus, such paths would not contribute to local multiple scattering. Average backscattering attenuation for all light paths that include a single backward scattering is

$$\bar{A}_1(\theta) = \bar{a}_b \sum_{i=1}^{\infty} \bar{a}_f^{2\,i} = \frac{\bar{a}_b\, \bar{a}_f^2}{1 - \bar{a}_f^2}\ , \quad (11)$$

where $\bar{a}_f(\theta)$ is the average forward scattering attenuation, and $\bar{a}_b(\theta)$ is the average backward scattering attenuation. It is computed similar to Equation 6 from fiber BCSDF for isotropic irradiance along the specular cone as

$$\bar{a}_b(\theta_d) = \frac{1}{\pi} \int_{\Omega_b} \int_{-\frac{\pi}{2}}^{\frac{\pi}{2}} f_s\left((\theta_d, \phi), \omega\right) \cos\theta_d \,\mathrm{d}\phi\,\mathrm{d}\omega, \quad (12)$$

[1] All hair fibers of a disciplined hair cluster share the same tangent

where Ω_b is all directions over the back hemisphere. In other words, we consider all paths for which light forward scatters through i fibers, then backward scatters once, then again forward scatters all the way back through the same i fibers. Note that the special case with no forward scattering ($i = 0$) is not included here, since it is handled separately within the single scattering computation.

The average backscattering attenuation for light paths with three backward scattering is approximated by the analytical solution of the following triple sum:

$$\bar{A}_3(\theta) = \bar{a}_b^3 \sum_{i=1}^{\infty} \sum_{j=0}^{i-1} \sum_{k=j+1}^{\infty} \bar{a}_f^{2(i-j-1+k)} = \frac{\bar{a}_b^3\, \bar{a}_f^2}{\left(1 - \bar{a}_f^2\right)^3}\ . \quad (13)$$

Here, we consider each possible case where light forward scatters through i fibers, backscatters, forward scatters through $j < i$ fibers, backscatters, and forward scatters through $k > j$ fibers before backscattering one last time and forward scattering all the way back through the $i - j - 1 + k$ fibers again. Since $\bar{a}_b(\theta)$ is small for human hair fibers, we disregard the paths with more than 3 backward scattering events, approximating the average backscattering attenuation as the sum of equations 11 and 13

$$\bar{A}_b(\theta) = \bar{A}_1(\theta) + \bar{A}_3(\theta)\ . \quad (14)$$

3.2.2 Average Backscattering Spread

Similar to the forward scattering spread function in Equation 7, we represent backscattering spread as the product of a constant azimuthal term $\tilde{s}_b$ and a Gaussian function for the longitudinal spread as

$$\bar{S}_b(\omega_i, \omega_o) = \frac{\tilde{s}_b(\phi_i, \phi_o)}{\cos\theta}\ g\Big(\ \theta_o + \theta_i - \bar{\Delta}_b(\theta)\ ,\ \bar{\sigma}_b^2(\theta)\ \Big)\ , \quad (15)$$

where $\tilde{s}_b(\phi_i, \phi_o)$ is $1/\pi$ for backward scattering directions and zero for forward scattering, $\bar{\Delta}_b(\theta)$ is the average longitudinal shift caused by the scattering events, and $\bar{\sigma}_b^2(\theta)$ is the average longitudinal variance for backscattering.

As in the computation of average backscattering attenuation, we consider all possible paths with one and three backward scattering events, and we compute average longitudinal shift using a weighted average of shifts due to all possible light paths

$$\bar{\Delta}_b = \frac{\bar{a}_b}{\bar{A}_b} \sum_{i=1}^{\infty} \bar{a}_f^{2i}\left(2i\bar{\alpha}_f + \bar{\alpha}_b\right) + \frac{\bar{a}_b^3}{\bar{A}_b} \sum_{i,j,k} \bar{a}_f^m\left(3\bar{\alpha}_b + m\bar{\alpha}_f\right),$$

where $\sum_{i,j,k}$ denotes $\sum_{i=1}^{\infty}\sum_{j=0}^{i-1}\sum_{k=j+1}^{\infty}$, m is $2(i-j-1+k)$, and $\bar{\alpha}_f(\theta)$ and $\bar{\alpha}_b(\theta)$ are average forward and backward scattering shifts, taken from the BCSDF of the hair fiber. Similarly, the average backscattering standard deviation is computed as

$$\bar{\sigma}_b = \frac{\bar{a}_b}{\bar{A}_b} \sum_{i=1}^{\infty} \bar{a}_f^{2i} \sqrt{2\,i\bar{\beta}_f^2 + \bar{\beta}_b^2} + \frac{\bar{a}_b^3}{\bar{A}_b} \sum_{i,j,k} \bar{a}_f^m \sqrt{3\,\bar{\beta}_b^2 + m\bar{\beta}_f^2},$$

where $\bar{\beta}_f^2(\theta)$ and $\bar{\beta}_b^2(\theta)$ are average forward and backward scattering variances of the hair fiber BCSDF. In these formulations, we approximate the sum of the Gaussian functions of the individual scattering spreads by a single Gaussian function with a combined mean ($\bar{\Delta}_b$) and standard deviation ($\bar{\sigma}_b$). This is a good approximation since for realistic hair BCSDF, longitudinal shifts are small and individual scattering lobes have a comparable standard deviation. In practice, we use the following analytical approximations[2]

[2] These analytical approximations are numerical fits based on a power series expansion with respect to $\bar{a}_b$ up to an order of three.

to these sums given above:

$$\bar{\Delta}_b \approx \bar{\alpha}_b \left(1 - \frac{2\bar{a}_b^2}{(1-\bar{a}_f^2)^2}\right) + \bar{\alpha}_f \left(\frac{2(1-\bar{a}_f^2)^2 + 4\bar{a}_f^2\bar{a}_b^2}{(1-\bar{a}_f^2)^3}\right) \quad (16)$$

$$\bar{\sigma}_b \approx \left(1 + 0.7\bar{a}_f^2\right) \frac{\bar{a}_b\sqrt{2\bar{\beta}_f^2 + \bar{\beta}_b^2} + \bar{a}_b^3\sqrt{2\bar{\beta}_f^2 + 3\bar{\beta}_b^2}}{\bar{a}_b + \bar{a}_b^3\left(2\bar{\beta}_f + 3\bar{\beta}_b\right)}. \quad (17)$$

3.3 General Rendering Equation

The equations we derived up to here assume that the hair model is illuminated by a single directional light source such that ω_d is constant. However, our formulation can be extended to arbitrary light sources as long as estimating all global scattering based on the shadow path is still practicable. We can rewrite the general form of the rendering equation incorporating the terms for global and local multiple scattering as

$$L_o(x,\omega_o) = \int_\Omega L_i^G(x,\omega_i)\, f(\omega_i,\omega_o)\, \cos\theta_i \,\mathrm{d}\omega_i\,, \quad (18)$$

where

$$L_i^G(x,\omega_i) = \int_\Omega L_d(x,\omega_d)\, \Psi^G(x,\omega_d,\omega_i)\,\mathrm{d}\omega_d \quad (19)$$

is the globally multiple scattered light entering the hair volume from all directions before scattering towards x in direction ω_i, and

$$f(\omega_i,\omega_o) = f_s(\omega_i,\omega_o) + d_b f_{back}(\omega_i,\omega_o) \quad (20)$$

is the BCSDF including both single hair fiber scattering and backscattering from a collection of fibers. Hence, this general rendering equation can handle multiple light sources, general shaped area lights, image based lighting from all directions, and full global illumination solution including multiple scattering in hair.

4 Implementation

For an efficient implementation of the dual scattering approximation we rewrite the general rendering equation, changing the order of the integrals in equations 18 and 19 as

$$L_o(x,\omega_o) = \int_\Omega L_d(x,\omega_d)\, F(x,\omega_d,\omega_o)\,\mathrm{d}\omega_d\,, \quad (21)$$

where

$$F(x,\omega_d,\omega_o) = \int_\Omega \Psi^G(x,\omega_d,\omega_i)\, f(\omega_i,\omega_o)\, \cos\theta_i \,\mathrm{d}\omega_i\,. \quad (22)$$

Since $L_d(x,\omega_d)$ is known (incoming radiance), all we need to compute is the function $F(x,\omega_d,\omega_o)$ to find the outgoing radiance. This computation has two main steps: the first step gathers the necessary information to compute the global multiple scattering function $\Psi^G(x,\omega_d,\omega_i)$ and the second one is the shading step that computes the above integral.

4.1 Computing Global Multiple Scattering

The global multiple scattering function can be computed in many different ways, with the choice of method determining the speed and accuracy of the overall implementation. Since global multiple scattering is estimated by analyzing a single prototype light path (along the shadow path), all implementations of global multiple scattering are very similar to different semi-transparent hair shadowing techniques. However, unlike these non-physical shadowing approaches that aim to compute a transmittance (or an opacity) function along the shadow path, in our dual scattering method we compute front scattering transmittance $T_f(x,\omega_d)$ and front scattering variance $\bar{\sigma}_f^2(x,\omega_d)$, along with the fraction of direct illumination that reaches the point of interest without being blocked (shadowed) by other hair strands.

4.1.1 Ray Shooting

Ray shooting is the simplest implementation of the global multiple scattering function. The procedure is very similar to ray traced shadow computation. To find the forward scattering transmittance and spread at point x due to illumination from direction ω_d, we shoot a ray from x in the direction ω_d. If the ray does not intersect with any hair strands, T_f is taken as 1, $\bar{\sigma}_f$ is set to zero, and the direct illumination fraction becomes 1. If there is an intersection with a hair strand, the direct illumination fraction becomes zero and we update the transmittance and variance values using equations 5 and 8. While computing the transmittance (Equation 5) we use a one dimensional lookup table for $\bar{a}_f(\theta_d)$, which is precomputed by numerical integration of Equation 6. The ray shooting method provides an accurate dual scattering approximation, however multiple ray samples per pixel are needed to eliminate sampling noise.

4.1.2 Forward Scattering Maps

To accelerate the global multiple scattering computation we implemented a two pass approach. We begin by generating a voxel grid that encloses the hair geometry. Each voxel in this grid keeps T_f and $\bar{\sigma}_f^2$ values along with a direct illumination fraction. In the first pass we trace rays from each light source towards the grid, computing T_f and $\bar{\sigma}_f^2$ values along the ray. The values of each voxel are determined by the average of the values along the rays that intersect with the voxel. In the second pass we render the hair geometry and find the global multiple scattering values using linear interpolation from the voxel grid. In our implementation we also applied multi-sampling to further smooth the results.

Using forward scattering maps significantly improves the rendering time as compared to the ray shooting method. Furthermore, this voxel grid can keep global multiple scattering information of multiple light sources within the same data structure; therefore, the performance gain of forward scattering maps becomes more significant as the number of light sources increase. On the other hand, the accuracy and performance of forward scattering maps depend on the map resolution (i.e. the extent of a voxel). For all examples presented in this paper the map resolution is 0.5 cm.

4.1.3 GPU Implementation

In our GPU implementation we used a similar approach to forward scattering maps based on the deep opacity maps method [Yuksel and Keyser 2008] developed for computing semi-transparent hair shadows. We chose the deep opacity maps method over other possible alternatives, since it generates high quality results with minimum computation and memory cost.

Similar to deep opacity maps, in the first pass we render a depth map from the light's point of view. This depth map is used in the second pass to shape the map layers conforming to the shape of the hair style. Therefore, the hair volume illuminated by the light source can be accurately sampled using a very small number of layers. In the third and final pass, we render the final hair image using the map to find the global multiple scattering values.

Instead of keeping a single opacity value for each map pixel as suggested by the deep opacity maps method, we store 7 values: T_f and $\bar{\sigma}_f$ values for each RGB color channel and the direct illumination fraction. Therefore, for every layer we need two textures to store all 7 values. Due to the efficiency of the deep opacity maps approach, we can achieve high quality results with as few as 4 layers, which are stored in 8 textures. The latest consumer graphics cards support generation of all these 8 textures in a single pass using multiple draw buffers. However, in our (earlier generation) GPU implementation we output 4 textures per pass and generate our maps using two passes (one additional pass as compared to the original deep opacity maps implementation).

4.2 Shading Computation

Once the global multiple scattering information is gathered, the shading step computes the rest of the integral in Equation 22. This step is the same for all implementations of dual scattering. We compute Equation 22 differently depending on whether or not the point x receives illumination directly without being blocked (shadowed) by other hair strands, which is determined by the direct illumination fraction value of the global multiple scattering information.

When point x receives illumination directly (i.e. no scattering events occur along the shadow path) the integral in Equation 22 evaluates to $f(\omega_d, \omega_o) \cos\theta_d$. Here $f(\omega_d, \omega_o)$ is the sum of the single scattering component and the average backscattering component f_{back} as given in Equation 20. The computation of the single scattering component is identical to [Marschner et al. 2003] and [Zinke et al. 2004], such that the longitudinal scattering function M, which is modeled as a Gaussian function, is multiplied by a precomputed azimuthal scattering function N. The backscattering component f_{back} is computed from Equation 10 using precomputed tables for $\bar{A}_b(\theta)$, $\bar{\Delta}_b(\theta)$, and $\bar{\sigma}_b^2(\theta)$.

When point x is blocked by other hair strands, it receives illumination via global multiple scattering. In this case the azimuthal forward scattering spread on x becomes isotropic and the longitudinal forward scattering spread is represented by a narrow Gaussian function as given in Equation 7. For efficient computation of Equation 22, instead of using numerical integration techniques, we approximate the result by combining azimuthal and longitudinal components of S_f and f. The combination of longitudinal components can be easily approximated for narrow Gaussian functions by using combined variances β_s^2 and β_{back}^2 for f_s and f_{back} respectively, such that

$$\beta_s^2(x, \omega_d, \omega_i) = \bar{\sigma}_f^2(x, \omega_d) + \beta^2(\theta) \text{ , and} \quad (23)$$

$$\beta_{\text{back}}^2(x, \omega_d, \omega_i) = \bar{\sigma}_f^2(x, \omega_d) + \bar{\sigma}_b^2(\theta) \text{ ,} \quad (24)$$

where $\beta^2(\theta)$ is the variance of the scattering lobe of the BCSDF[3]. In the azimuthal direction, f_{back} is already isotropic; therefore, isotropic forward scattering does not affect this component. However, the azimuthal component N of f_s changes under isotropic azimuthal irradiance. We precompute this component N^G and store it in a 2D table similar to N using numerical integration of

$$N^G(\theta, \phi) = \int_{-\frac{\pi}{2}}^{\frac{\pi}{2}} \tilde{s}_f(\phi)\, N(\theta, \phi')\, \mathrm{d}\phi' \text{ .} \quad (25)$$

Note that this formulation ignores the elipticity of hair fibers. However, this approximation is still accurate enough even for elliptic hair fibers, since $\tilde{s}_f = 1/\pi$ is isotropic (constant) and N^G is averaging f_s along the front half cone.

[3]The BCSDF has three lobes, one for each component: R, TT, and TRT

Table 1: *Precomputed tables used for shading*

Function	Reference	Use
$\bar{A}_b(\theta)$	Equation 14	local multiple scattering
$\bar{\Delta}_b(\theta)$	Equation 16	local multiple scattering
$\bar{\sigma}_b^2(\theta)$	Equation 17	local multiple scattering
$N^G(\theta, \phi)$	Equation 25	BCSDF due to forward scattering

$\mathbf{F}(T_f, \bar{\sigma}_f^2, \text{directFraction})$

// Compute local multiple scattering contribution

$f_{\text{back}} \leftarrow 2\, \bar{A}_b(\theta)\, g(\theta_d + \theta_o - \bar{\Delta}_b(\theta), \bar{\sigma}_b^2(\theta) + \bar{\sigma}_f^2)/(\pi\, \cos^2\theta)$

// Compute BCSDF of the fiber due to direct illumination

$M_{\text{R,TT,TRT}} \leftarrow g(\theta - \alpha_{\text{R,TT,TRT}}, \beta_{\text{R,TT,TRT}}^2)$

$f_s^{\text{direct}} \leftarrow M_{\text{R}} N_{\text{R}}(\theta, \phi) + M_{\text{TT}} N_{\text{TT}}(\theta, \phi) + M_{\text{TRT}} N_{\text{TRT}}(\theta, \phi)$

$F^{\text{direct}} \leftarrow \text{directFraction} \left(f_s^{\text{direct}} + d_b\, f_{\text{back}} \right)$

// Compute BCSDF of the fiber due to forward scatterd illumination similarly

$M^G_{\text{R,TT,TRT}} \leftarrow g(\theta - \alpha_{\text{R,TT,TRT}}, \beta_{\text{R,TT,TRT}}^2 + \bar{\sigma}_f^2)$

$f_s^{\text{scatter}} \leftarrow M_{\text{R}}^G N_{\text{R}}^G(\theta, \phi) + M_{\text{TT}}^G N_{\text{TT}}^G(\theta, \phi) + M_{\text{TRT}}^G N_{\text{TRT}}^G(\theta, \phi)$

$F^{\text{scatter}} \leftarrow (T_f - \text{directFraction})\; d_f \left(f_s^{\text{scatter}} + \pi d_b\, f_{\text{back}} \right)$

// Combine direct and forward scattered components

return $(F^{\text{direct}} + F^{\text{scatter}}) \cos\theta_i$

Figure 5: *Pseudo code of our dual scattering shader. α and β values are measured hair characteristics (part of the BCSDF) and computation of M and N is discussed in Section 2.2. Other precomputed tables are given in Table 1.*

To accelerate most computations we use small precomputed tables that store complicated hair fiber properties. These tables are listed in Table 1. The precomputations are simply numerical integrations of the given equations. In addition to these tables, we use a precomputed table for the azimuthal part of single fiber scattering, $N(\theta, \phi)$, which can be computed using techniques described in [Marschner et al. 2003] or [Zinke and Weber 2007].

Figure 5 shows the pseudo code for computing Equation 22 using this procedure. This pseudo code is a simple extension to the BCSDF shading computation; therefore, our method can be easily integrated into existing physically based hair rendering systems.

5 Results

To test the validity of our simplifications, we compared the results of our dual scattering approximation directly to path tracing. Figure 6 shows such a comparison for a disciplined cluster of blond hair, where the single scattering component is excluded to compare the results of multiple scattering only. As can be seen from these images, our approximation generates very similar results to path tracing regardless of the incident light direction. Although there are subtle differences compared to the results obtained with unbiased path tracing, the general look is very similar and irregularities that occur in real hairstyles tend to conceal such errors.

The graph in Figure 7 shows the comparison of radiance values in the middle of the clusters in Figure 6. Here, the average BRDF of multiple scattered light is shown for longitudinal and azimuthal sweeps along the cluster for various absorption coefficients. As can be seen from this graph, the azimuthal component of backward scattering (white region of the left graph) is almost isotropic, while the longitudinal component resembles a Gaussian distribution as modeled in our formulation. Even though the approximation slightly overshoots the accurate simulation for very low coefficients, the results indicate that our approach is a viable approximation for scattering from a cluster.

We also tested the accuracy of our dual scattering method for differ-

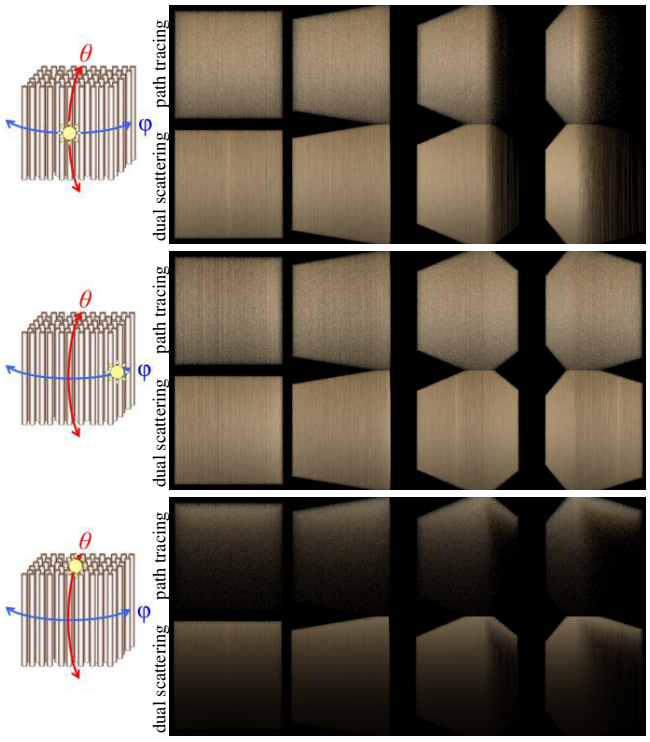

Figure 6: *Comparison (multiple scattering only) of dual scattering using ray shooting to path tracing for a cube shaped disciplined hair cluster consisting of 64K hair fibers illuminated by a single directional light source (light direction is shown on the left).*

ent hair fiber scattering properties. Figure 8 and Figure 9 show that dual scattering provides a good approximation for various hair colors and longitudinal Gaussian widths (standard deviations). Slight changes of the optical properties of a fiber (such as absorption) may have a drastic impact on the overall hair color. As can been in these figures, our approximation handles such variations correctly.

Despite the common intuition, it is more difficult to perceive errors in complicated models (where detail can hide problems), while even the slightest errors show up on simple models. We show a complicated hair model example in Figure 10. Since dual scattering only exploits local symmetry in the hair model, most of our assumptions still hold and we can produce a close approximation to the path tracing reference with significantly improved rendering times.

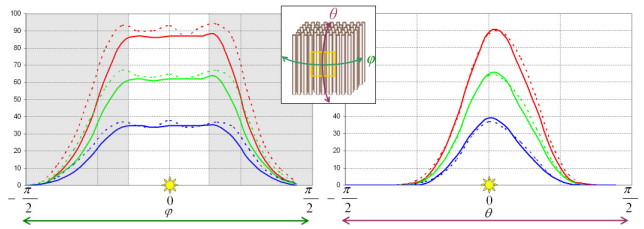

Figure 7: *The average BRDF (multiple scattering only) at a blond hair cluster computed for the red, green and blue components of light blond hair (see Figure 6) using path tracing (solid lines) and dual scattering approximation (dashed lines). The scene is illuminated by a directional front light source which means that for $\phi \approx 0$ (white area) the results are dominated by purely local multiple scattering (f_{back}) since no visible fibers are shadowed.*

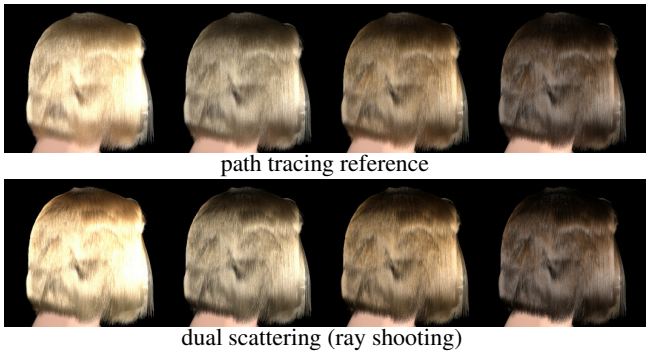

Figure 8: *Comparison for various hair colors with RGB absorption coefficients (from left to right) (0.03,0.07,0.15), (0.15,0.2,0.3), (0.2,0.3,0.5), and (0.3,0.6,1.2).*

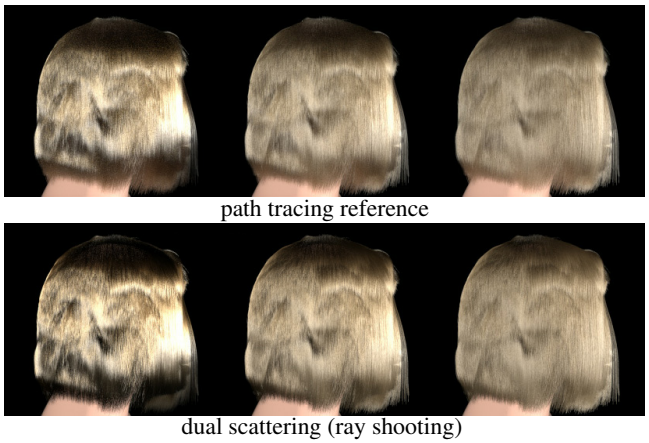

Figure 9: *Comparison for varying longitudinal widths β_R, β_{TT}, and β_{TRT} of the BCSDF (from left to right) (4, 5, 7.5), (8, 10, 15), (16, 20, 30)*

Figure 11 compares the offline implementations of dual scattering to path tracing and single scattering as well as to photon mapping (using ray based global illumination [Zinke and Weber 2006]) techniques. As can be seen from these images, while single scattering produces a dark image that fails to reproduce the correct color of hair, all other methods produce similar results to path tracing, while offline implementations of dual scattering significantly improve the rendering speed.

Figure 12 presents captured frames from our GPU based implementation of dual scattering, and comparisons to offline dual scattering (ray shooting) and path tracing. The figure shows three scattering components (single, global multiple, and local multiple) that produce the full dual scattering solution when combined. For this hair style the performance of the GPU implementation of dual scattering (12 fps) is comparable to the performance of a deep opacity maps [Yuksel and Keyser 2008] implementation (18 fps). Using extended multiple draw buffers, the additional pass we use for GPU-based dual scattering can be eliminated, which would significantly reduce the performance gap between our method and existing non-physical real-time solutions.

6 Discussion and Conclusion

Dual scattering offers a physically based simplification to the complicated phenomenon of multiple scattering in hair, exploiting scattering properties of hair fibers (such as narrow scattering along longitudinal directions and wide scattering along azimuthal directions) and general characteristics of human hair models (such as local sim-

Single Scattering Only (offline) 3 minutes	Path Tracing Reference (offline) 22 hours	**Dual Scattering** (ray shooting) 9.6 minutes	**Dual Scattering** (forward scattering map) 4.6 minutes	**Dual Scattering** (GPU-based) 5.8 fps

Figure 10: *Comparison of our dual scattering approximation method to path tracing ("ground truth") for a complicated hair style with 50K strands and 3.4M segments. The hair model is illuminated by two light sources, one of which act as a back light.*

0.0 0.1 0.2 0.3 0.4 0.5 **0.6** **0.7** **0.8** 0.9 1.0

Figure 13: *The effect of forward and backward scattering density factors $d_f(x, \omega_d)$ and $d_b(x, \omega_d)$. Values of 0.0 are equivalent to single scattering only. For most human hair styles values between 0.6 and 0.8 generate close approximations to path tracing.*

ilarity of fiber directions). By splitting multiple scattering into a local and a global part and using different approximations regarding the directionality of scattering from hair fibers, our dual scattering approach is orders of magnitude faster than other accurate techniques. We justify our simplifications by not only the theory but also several comparisons to ground truth (path tracing) in both experimental setups and realistic cases.

It is important to note that all of the computations described rely on physically-based values. All parameters are either fundamental to the virtual scene (e.g. directions such as ω_i), or are characteristics of real hair that can be accurately measured and described (e.g. the α and β values, and the BCSDF description). The only "user adjustable" term is the density factor (d_f and d_b), but even this has a physical meaning that limits the range of choices and, in theory, it could be computed precisely. Figure 13 shows the effect of changing density parameters.

The multiple scattering computation simplifications introduced in this paper are based on theoretical approximations rather than ad-hoc appearance-based formulations. As a result, despite the aggressive simplifications we have made, we obtain close approximations with no parameter adjustment and much faster computations.

On the other hand, one can come up with special hair models that would break some of our assumptions. For instance, if the mean path length is large (as in sparse hairstyles) or if attenuation coefficients are very small, the global structure of a hairstyle tends to play an important role that biases the results. Furthermore, the assumption that neighboring hair strands exhibit a similar structure can be violated in chaotic hair models. However, even for complicated cases our results look plausible and close to reference images with significantly improved computation times.

One limitation of our formulation arises from the fact that we use the shadow path as a prototype for all significant multiple scattered paths. Therefore, when there is a strong spatial variation in illumination, this prototype path assumption may be violated. For example, a hard shadow edge falling across the hair creates a sharp illumination change, hence our prototype path approximation would be less accurate along the shadow boundary.

We believe that separating local and global multiple scattering is a very general principle that is applicable not only in the realm of hair rendering, but also for other highly scattering quasi-homogeneous structures such as snow, clouds or woven textiles.

Acknowledgements

We would like to thank Murat Afsar for the head model, and Anton Andriyenko for the hair model in Figures 8, 9 and 11. We would also like to thank the anonymous reviewers for their helpful comments. This work is supported in part by *NSF* grant CCR-0220047 and *Deutsche Forschungsgemeinschaft* under grant We1945/3-2.

References

BERTAILS, F., MÉNIER, C., AND CANI, M.-P. 2005. A practical self-shadowing algorithm for interactive hair animation. In *Graphics Interface*, 71–78.

GUPTA, R., AND MAGNENAT-THALMANN, N. 2005. Scattering-based interactive hair rendering. In *Comp. Aided Design and Comp. Graphics*, 489–496.

HADWIGER, M., KRATZ, A., SIGG, C., AND BÜHLER, K. 2006. Gpu-accelerated deep shadow maps for direct volume rendering. In *Proceedings of Graphics Hardware 2006*, 49–52.

KIM, T.-Y., AND NEUMANN, U. 2001. Opacity shadow maps. In *Eurographics Rendering Workshop*, 177–182.

KNISS, J., PREMOZE, S., HANSEN, C., SHIRLY, P., AND MCPHERSON, A. 2003. A model for volume lighting and modeling. *IEEE Trans. on Vis. and Comp. Graphics 9*, 2, 150–162.

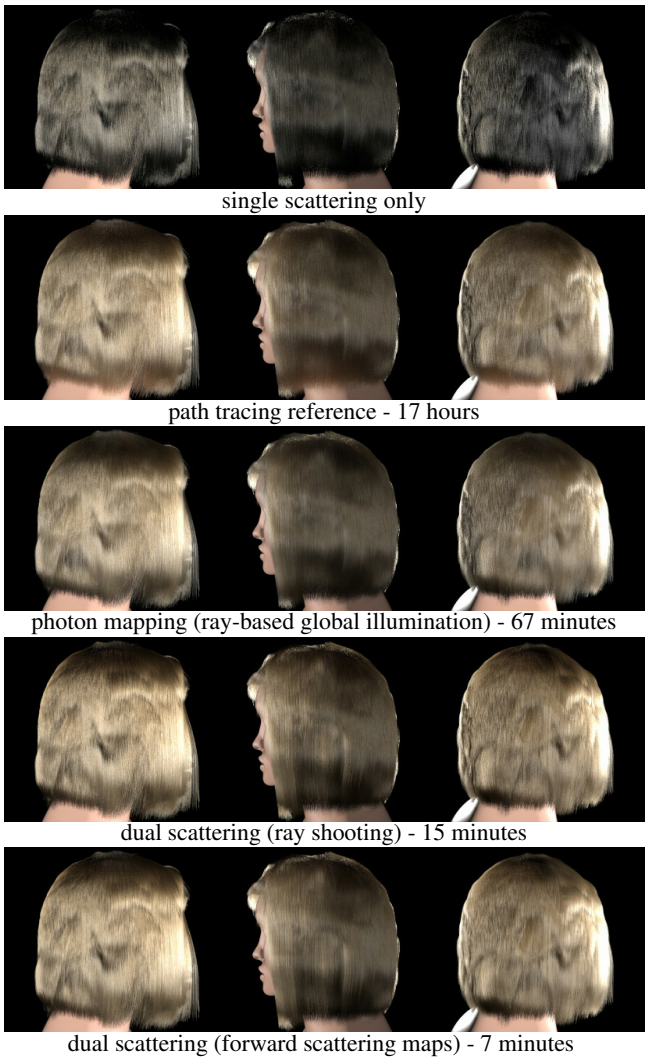

Figure 11: *Comparison of a blond hairstyle (87K strands) viewed from three different perspectives (illuminated by three directional light sources).*

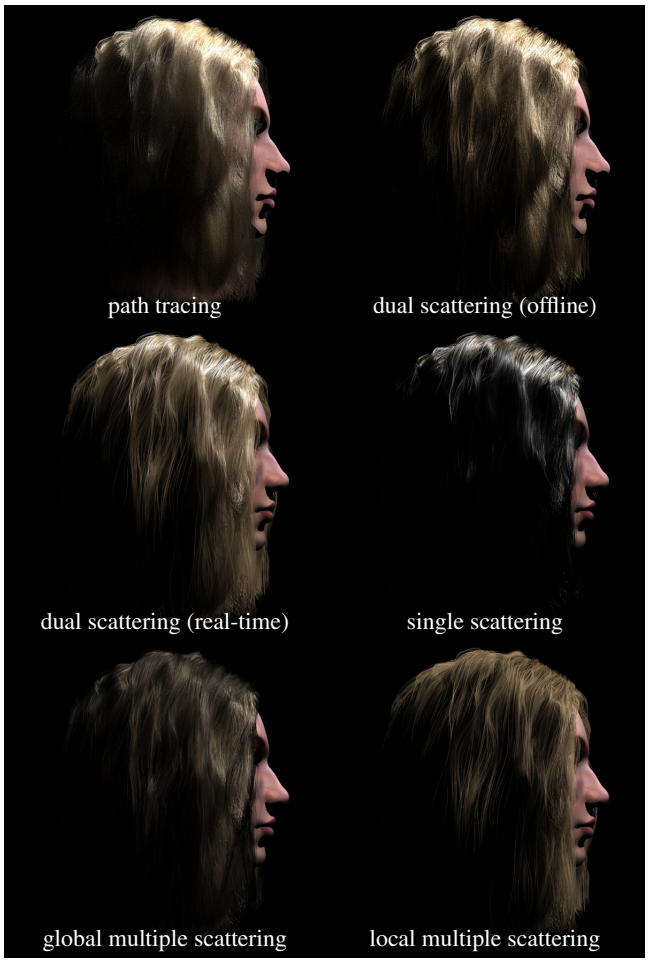

Figure 12: *Components of dual scattering method captured from our real-time implementation (12 fps) and comparisons to offline dual scattering using ray shooting (11.2 minutes) and path tracing reference (11.8 hours). The hair model has 50K strands and 2.4M line segments.*

LOKOVIC, T., AND VEACH, E. 2000. Deep shadow maps. In *Proceedings of SIGGRAPH 2000*, 385–392.

MARSCHNER, S. R., JENSEN, H. W., CAMMARANO, M., WORLEY, S., AND HANRAHAN, P. 2003. Light scattering from human hair fibers. *ACM Transactions on Graphics 22*, 3, 780–791. SIGGRAPH 2003.

MERTENS, T., KAUTZ, J., BEKAERT, P., AND REETH, F. V. 2004. A self-shadow algorithm for dynamic hair using density clustering. In *Eurographics Symposium on Rendering*, 173–178.

MOON, J. T., AND MARSCHNER, S. R. 2006. Simulating multiple scattering in hair using a photon mapping approach. *ACM Transactions on Graphics 25*, 3, 1067–1074. SIGGRAPH 2006.

PREMOZE, S., ASHIKHMIN, M., RAMAMOORTHI, R., AND NAYAR, S. 2004. Practical rendering of multiple scattering effects in participating media. In *Eurographics Symp. on Rendering*.

WARD, K., BERTAILS, F., KIM, T.-Y., MARSCHNER, S. R., CANI, M.-P., AND LIN, M. 2007. A survey on hair modeling: Styling, simulation, and rendering. *IEEE Transactions on Visualization and Computer Graphics 13*, 2, 213–34.

XU, S., LAU, F. C., JIANG, H., AND PAN, Y. 2006. A novel method for fast and high-quality rendering of hair. In *Proc. of the 17th Eurographics Symp. on Rendering*, 331–341, 440.

YUKSEL, C., AND KEYSER, J. 2008. Deep opacity maps. *Computer Graphics Forum (Proc. of EUROGRAPHICS 2008) 27*, 2.

YUKSEL, C., AKLEMAN, E., AND KEYSER, J. 2007. Practical global illumination for hair rendering. In *Pacific Graphics 2007*, 415–418.

ZINKE, A., AND WEBER, A. 2006. Global illumination for fiber based geometries. In *Electronic proceedings of the Ibero American Symposium on Computer Graphics (SIACG 2006)*.

ZINKE, A., AND WEBER, A. 2007. Light scattering from filaments. *IEEE Trans. on Vis. and Comp. Graphics 13*, 2, 342–356.

ZINKE, A., SOBOTTKA, G., AND WEBER, A. 2004. Photorealistic rendering of blond hair. In *Vision, Modeling, and Visualization (VMV) 2004*, 191–198.